

Article

Study on the Visible-Light Photocatalytic Performance and Degradation Mechanism of Diclofenac Sodium under the System of Hetero-Structural $\text{CuBi}_2\text{O}_4/\text{Ag}_3\text{PO}_4$ with H_2O_2

Xiaojuan Chen ¹, Ning Li ^{1,2,*}, Song Xu ¹, Hailong Wang ^{1,3}  and Yumin Cai ¹

¹ School of Environment and Chemical Engineering, Foshan University, Foshan 528000, China; xjchen0218@163.com (X.C.); xuson@yeah.net (S.X.); nzhailongwang@163.com (H.W.); cym0171@126.com (Y.C.)

² College of Marine Sciences, Sun Yat-sen University, Guangzhou 510275, China

³ Key Laboratory of Soil Contamination Bioremediation of Zhejiang Province, Zhejiang A & F University, Hangzhou 311300, China

* Correspondence: lining43@mail.sysu.edu.cn; Tel.: +86-757-8278-7103

Received: 19 February 2018; Accepted: 27 March 2018; Published: 28 March 2018



Abstract: Two kinds of $\text{CuBi}_2\text{O}_4/\text{Ag}_3\text{PO}_4$ with different heterojunction structures were prepared based on the combination of hydrothermal and in-situ precipitation methods with surfactant additives (sodium citrate and sodium stearate), and their characteristics were systematically resolved by X-ray Diffraction (XRD), Brunauer–Emmett–Teller (BET), X-ray Photoelectron Spectroscopy (XPS), Scanning Electron Microscope (SEM)/ High-resolution Transmission Electron Microscopy (HRTEM), UV-vis Diffuse Reflectance Spectra (DRS) and Photoluminescence (PL). Meanwhile, the photocatalytic properties of the catalysts were determined for diclofenac sodium (DS) degradation and the photocatalytic mechanism was also explored. The results indicate that both of the two kinds of $\text{CuBi}_2\text{O}_4/\text{Ag}_3\text{PO}_4$ exhibit higher photocatalytic efficiency, mineralization rate, and stability than that of pure CuBi_2O_4 or Ag_3PO_4 . Moreover, the catalytic activity of $\text{CuBi}_2\text{O}_4/\text{Ag}_3\text{PO}_4$ can be further enhanced by adding H_2O_2 . The free radical capture experiments show that in the pure $\text{CuBi}_2\text{O}_4/\text{Ag}_3\text{PO}_4$ photocatalytic system, the OH^\bullet and $\text{O}_2^{\bullet-}$ are the main species participating in DS degradation; however, in the $\text{CuBi}_2\text{O}_4/\text{Ag}_3\text{PO}_4$ photocatalytic system with H_2O_2 , all OH^\bullet , h^+ , and $\text{O}_2^{\bullet-}$ take part in the DS degradation, and the contribution order is $\text{OH}^\bullet > h^+ > \text{O}_2^{\bullet-}$. Accordingly, the photocatalytic mechanism of $\text{CuBi}_2\text{O}_4/\text{Ag}_3\text{PO}_4$ could be explained by the Z-Scheme theory, while the catalysis of $\text{CuBi}_2\text{O}_4/\text{Ag}_3\text{PO}_4$ with H_2O_2 follows the heterojunction energy band theory.

Keywords: CuBi_2O_4 ; Ag_3PO_4 ; H_2O_2 ; heterojunction; visible-light; stability

1. Introduction

Diclofenac sodium (DS) is a typical non-steroidal anti-inflammatory drug [1–3]. The usage of DS in China amounts to thousands of tonnes every year. Because of the strong water solubility of DS and its poor absorption by organisms, most of the DS intake by human and animals is excreted through feces and urine in the form of parent or active metabolites, finally flowing into the aquaculture wastewater and municipal wastewater [4]. Numerous studies have indicated that only less than 20% of DS can be removed from the traditional sewage treatment plant. Therefore, the DS, which enters the environment with effluent water, not only causes a serious poisoning effect on aquatic organisms, but also poses a significant threat to other living beings and human health through food

chain accumulation [4,5]. Based on this, the effective degradation technologies for DS must be explored to control its continued contamination.

Photocatalytic technology had aroused widespread concern in the field of organic pollutant treatment due to the advantages of mild reaction conditions, fast reaction speed, high mineralization rate, and less secondary pollution [6–10]. Moreover, photocatalysts are the main body of photocatalytic technology, which play a decisive role in the photocatalytic activity of the reaction system [11,12]. To make full use of the visible light spectrum that occupies 43% of the clean solar energy, the current research and development mainly focuses on the visible light-responsive photocatalysts. Silver phosphate (Ag_3PO_4), which can absorb sunlight with wavelength less than 520 nm, is a visible light-responsive photocatalyst discovered in 2010 [11,13]. It exhibits high quantum yield and excellent photocatalytic activity. However, the Ag^+ on the surface of Ag_3PO_4 can be easily reduced to be Ag^0 ($4\text{Ag}_3\text{PO}_4 + 6\text{H}_2\text{O} + 12h^+ + 12e^- \rightarrow 12\text{Ag}^0 + 4\text{H}_3\text{PO}_4 + 3\text{O}_2$) in the pure Ag_3PO_4 photocatalytic reaction system [11,14,15]. This is due to the slight solubility of Ag_3PO_4 in solution (solubility of 0.02 g/L) and the higher electrode potential of Ag/Ag^+ than the conduction band potential of Ag_3PO_4 , causing the photo-corrosion. The photo-corrosion destroys the stability of Ag_3PO_4 and decreases its photocatalytic activity, finally leading to the inactivation of Ag_3PO_4 .

Related studies have shown that the hetero-structural photocatalysts, which can be constructed by combination of Ag_3PO_4 and other semiconductor materials, not only can promote the separation of photogenerated electron-hole pairs through belt matching with each other, but also can optimize the photocatalytic activity and stability of Ag_3PO_4 through transformation and being captured by electrons [16–20]. CuBi_2O_4 is another visible light-responsive photocatalyst, although its quantum yield is low, it poses good chemical stability, high conduction band position, and strong reducing ability [21–23]. Currently, CuBi_2O_4 is mainly used for fluorescent and photocathode materials [24,25], and its application in the field of photocatalytic oxidation technology has been rarely reported. Based on the band structure characteristics of Ag_3PO_4 and CuBi_2O_4 , heterojunction photocatalyst of $\text{CuBi}_2\text{O}_4/\text{Ag}_3\text{PO}_4$ should have excellent photocatalytic properties compared with the pure catalysts, including activity and stability.

Therefore, in this study, a combination of hydrothermal and in-situ precipitation methods were used to construct two kinds of hetero-structural photocatalysts $\text{CuBi}_2\text{O}_4/\text{Ag}_3\text{PO}_4$ by adding different surfactants of sodium citrate or sodium stearate in the preparation systems, which can be respectively named as $\text{CuBi}_2\text{O}_4/\text{Ag}_3\text{PO}_4\text{-SC}$ and $\text{CuBi}_2\text{O}_4/\text{Ag}_3\text{PO}_4\text{-SS}$. As a comparison, the pure Ag_3PO_4 with the additives of sodium citrate or sodium stearate are recorded as $\text{Ag}_3\text{PO}_4\text{-SC}$ and $\text{Ag}_3\text{PO}_4\text{-SS}$, respectively. Then, the physical and chemical properties of the as-prepared materials were systematically characterized, and their photocatalytic activity and stability under visible light irradiation were also evaluated for DS degradation. Moreover, the effect of H_2O_2 on the catalytic property and mechanism of $\text{CuBi}_2\text{O}_4/\text{Ag}_3\text{PO}_4$ was also comprehensively investigated.

2. Materials and Methods

2.1. Materials

All reactants and solvents were analytical grade and used without further purification. AgNO_3 , $\text{Na}_2\text{HPO}_4 \cdot 12\text{H}_2\text{O}$, $\text{Bi}(\text{NO}_3)_3 \cdot 5\text{H}_2\text{O}$, $\text{Cu}(\text{NO}_3)_2 \cdot 3\text{H}_2\text{O}$, H_2O_2 , sodium citrate (Na_3Cit), sodium stearate ($\text{C}_{17}\text{H}_{35}\text{COONa}$), tert-butanol (*t*-BuOH), para-benzoquinone (BZQ), disodium ethylenediaminetetra-acetate ($\text{Na}_2\text{-EDTA}$), ethanol, and diclofenac sodium were obtained from Sinopharm Chemical Reagent Co., Ltd., (Shanghai, China). Ultrapure water was used throughout this study.

2.2. Preparation of Hetero-Structural $\text{CuBi}_2\text{O}_4/\text{Ag}_3\text{PO}_4$

CuBi_2O_4 was first synthesized through the hydrothermal synthesis method, and the detailed processes are as follows. Simply speaking, 1.3582 g $\text{Bi}(\text{NO}_3)_3 \cdot 5\text{H}_2\text{O}$ was adequately dissolved into

HNO₃. Next, 20 mL of Cu(NO₃)₂·3H₂O (0.3382 g) was added into the above solution mechanically and agitated for 30 min. Then the precipitator NaOH (1.2 M, 20 mL) was added to the reaction system drop by drop. After the solution was diluted to 70 mL, the mixture was transferred into a sealed Teflon-lined stainless steel autoclave of 100 mL and reacted at 100 °C for 24 h under autogenous pressure. The precipitates were isolated by centrifugation when the autoclave was cooled naturally to room temperature; finally, the solids were washed several times with distilled water and dried at 60 °C for 24 h.

The CuBi₂O₄/Ag₃PO₄ composites with different hetero-structures were prepared through an in-situ deposition process by adding different surfactants of sodium citrate or sodium stearate into the preparation systems. The detailed preparation process is as following. An amount of 0.1 g of CuBi₂O₄ prepared above was first dispersed in 40 mL of ultrapure water and ultrasonically treated at 100 W for 15 min, then 10 mL of sodium citrate (or sodium stearate) solution was added into the reaction system and mechanically agitated for 2 h. After that, 10 mL of AgNO₃ solution was added into the mixture. After further stirring for 30 min, 20 mL of Na₂HPO₄·12H₂O was added dropwise into the system. The precipitate was isolated and washed several times with absolute ethanol and distilled water, then dried at 60 °C overnight. According to the added surfactants of sodium citrate or sodium stearate, two kinds of CuBi₂O₄/Ag₃PO₄ can be obtained, and the products can be respectively named as CuBi₂O₄/Ag₃PO₄-SC (wt:wt = 3:7) and CuBi₂O₄/Ag₃PO₄-SS (wt:wt = 1:1). As a comparison, the pure Ag₃PO₄ with the additives of sodium citrate or sodium stearate are recorded as Ag₃PO₄-SC and Ag₃PO₄-SS, respectively.

2.3. Characterization

Powder X-ray diffraction (XRD, D/MAX-2500/PC) was used to examine the crystalline phase of the products, and each sample was scanned through a 2θ range of 10–90° at a rate of 4°/min. The nitrogen adsorption-desorption isotherms of the photocatalysts were obtained using an NOVA-2200e volumetric analyzer (Quantachrome, Boynton Beach, FL, USA), and the surface areas of the samples estimated by the BET model. The morphology of the samples was obtained by scanning electron microscopy (SEM, JSM-6610LV, JOEL, Tokyo, Japan) and high-resolution transmission electron microscopy (HRTEM, Tecnai G² F20 S-TWIN, FEI, Hillsboro, OR, USA). The ultraviolet-visible diffuse reflectance spectra were obtained using a scanning UV-Vis spectrophotometer (UV-2550, Shimadzu, Kyoto, Japan) within a range of 200–800 nm. Additionally, the X-ray photoelectron spectra (XPS, ESCALAB 250, Thermo Scientific, Waltham, MA, USA) were recorded with Al K α radiation to investigate the content of Ag⁰ in the fresh and reused catalysts. The photoluminescence (PL) spectroscopy was performed using a fluorescence spectrophotometer (FP-6500, JASCO, Oklahoma City, OK, USA).

2.4. Photocatalytic Performance Measurement

The photocatalytic activity of the as-prepared materials was evaluated for DS degradation, and the reaction apparatus was a photocatalytic reactor (BL-GHX-V, Bilang Biological Science and Technology Co., Ltd., Xi'an, China) using a 300 W Xe lamp with an ultraviolet cutoff filter (providing visible light ≥ 400 nm) as the light source. In each experiment, 30 mg of photocatalyst was added to a 50 mL DS solution at an initial concentration of 15 mg/L. Prior to illumination, the solution was magnetically stirred in the dark for 30 min to reach the adsorption-desorption equilibrium between the DS and photocatalysts. Then, the solution was exposed to Xe lamp irradiation. At a given time interval of irradiation, one reaction tube was taken out and magnetically separated to remove the catalyst. Finally, the supernatant was withdrawn and filtered with 0.45 μ m membrane filters. The concentration of DS and TOC were measured by high efficiency liquid chromatography (HPLC, Agilent 1260, Santa Clara, CA, USA) and a TOC (Shimadzu TOC-V_{CPH}, Kyoto, Japan) analyzer, respectively. To determine the effect of H₂O₂ on the catalytic performance of CuBi₂O₄/Ag₃PO₄, different concentrations of H₂O₂ were added to the reaction system in the early stage, while the other

experimental steps were the same as for the photocatalytic activity. In addition, the repeated experiments for DS degradation were also conducted to study the stability of the as-prepared photocatalysts, and the operation processes were also similar to the photocatalytic experiments.

2.5. Analysis of Reactive Species

Free radical capture experiments were used to ascertain the reactive species for DS photodegradation, and tert-butanol (*t*-BuOH) was chosen as the hydroxyl radical (OH^\bullet) scavenger, disodium ethylenediamine tetra-acetate (EDTA-Na_2) was chosen as the hole (h^+) scavenger, benzoquinone (BZQ) was chosen as the superoxide radical ($\text{O}_2^{\bullet-}$) scavenger. The detailed free radical capture experiment processes were similar to the photocatalytic activity experiments.

3. Results

3.1. Characterizations

Figure 1 shows the XRD patterns of the synthesized photocatalysts of CuBi_2O_4 , $\text{Ag}_3\text{PO}_4\text{-SC}$, $\text{Ag}_3\text{PO}_4\text{-SS}$, $\text{CuBi}_2\text{O}_4/\text{Ag}_3\text{PO}_4\text{-SC}$, and $\text{CuBi}_2\text{O}_4/\text{Ag}_3\text{PO}_4\text{-SS}$. It can be seen that the diffraction peaks in the XRD pattern of pure CuBi_2O_4 can be perfectly indexed to the phase of CuBi_2O_4 (JCPDS No. 84-1969) [26], and the reflections at $2\theta = 20.48^\circ$, 27.73° , 30.76° , 32.73° , 34.20° , 37.30° , 46.04° , 53.02° , 55.08° , 59.94° , and 65.92° are attributed to the crystal planes of (200), (211), (002), (310), (102), (202), (411), (213), (332), (521), and (413), respectively. For the XRD patterns of $\text{Ag}_3\text{PO}_4\text{-SC}$ and $\text{Ag}_3\text{PO}_4\text{-SS}$, all the diffraction peaks correspond to the standard card of Ag_3PO_4 (JCPDS No.06-0505) [13]. In addition, as can be seen from the XRD patterns of $\text{CuBi}_2\text{O}_4/\text{Ag}_3\text{PO}_4\text{-SC}$ and $\text{CuBi}_2\text{O}_4/\text{Ag}_3\text{PO}_4\text{-SS}$, the diffraction peaks only indicate CuBi_2O_4 or Ag_3PO_4 , with absence of any other substances, indicating that Ag_3PO_4 couples with CuBi_2O_4 mainly through physical effects, but not chemical reaction.

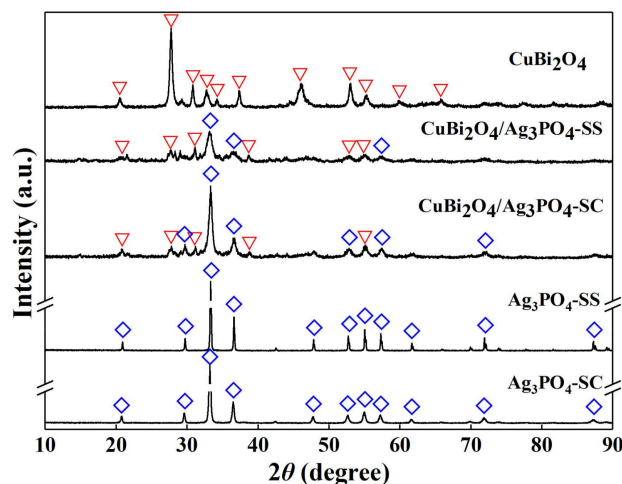


Figure 1. Powder X-ray diffraction (XRD) patterns of the as-prepared photocatalysts.

The SEM images of as-prepared photocatalysts of CuBi_2O_4 , $\text{Ag}_3\text{PO}_4\text{-SC}$, $\text{Ag}_3\text{PO}_4\text{-SS}$, $\text{CuBi}_2\text{O}_4/\text{Ag}_3\text{PO}_4\text{-SC}$, and $\text{CuBi}_2\text{O}_4/\text{Ag}_3\text{PO}_4\text{-SS}$ are shown in Figure 2. Apparently, from Figure 2a, pure CuBi_2O_4 presented a spherical structure with good dispersibility and smooth surface, its diameter is about 5 μm . Figure 2b displays the micro-topography structure of $\text{Ag}_3\text{PO}_4\text{-SC}$ using sodium citrate as additive, and the products exhibit irregular spheres of about 500–800 nm in diameter. If the additive of sodium stearate is used in the preparation system of Ag_3PO_4 , the product $\text{Ag}_3\text{PO}_4\text{-SS}$ shown in Figure 2c behaves with a smaller diameter of about 200–600 nm as irregular spheres. Figure 2d, indicating the SEM and HRTEM images of $\text{CuBi}_2\text{O}_4/\text{Ag}_3\text{PO}_4\text{-SC}$, demonstrates the composite material contains two kinds of spherical structure with different diameters, and the substances are CuBi_2O_4

and Ag_3PO_4 by comparison with the SEM images of pure CuBi_2O_4 and Ag_3PO_4 -SC. Moreover, a heterojunction has formed due to the close contact between CuBi_2O_4 and Ag_3PO_4 . However, as for the $\text{CuBi}_2\text{O}_4/\text{Ag}_3\text{PO}_4$ -SS, whose SEM and HRTEM images are shown in Figure 2e, only one spherical structure with rough surface and diameter of about 5–6 μm is obtained, indicating the nano particulates Ag_3PO_4 are attached onto the surface of CuBi_2O_4 and a complete heterojunction composite is formed.

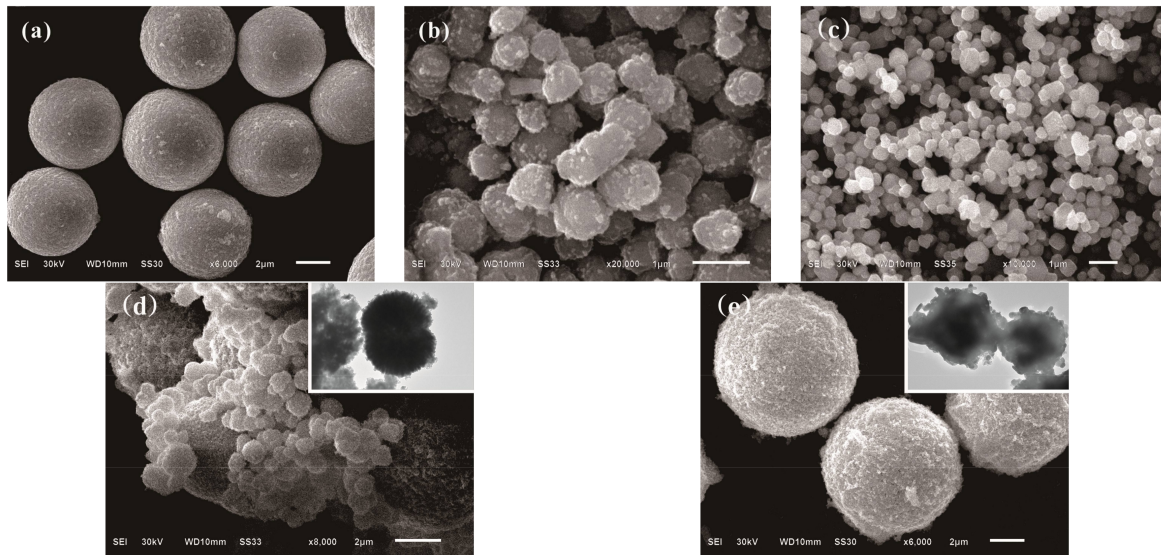


Figure 2. Scanning electron microscopy (SEM) images of photocatalysts, (a) CuBi_2O_4 ; (b) Ag_3PO_4 -SC; (c) Ag_3PO_4 -SS; (d) $\text{CuBi}_2\text{O}_4/\text{Ag}_3\text{PO}_4$ -SC; (e) $\text{CuBi}_2\text{O}_4/\text{Ag}_3\text{PO}_4$ -SS. The illustrations in (d,e) indicate the high-resolution transmission electron microscopy (HRTEM) images of $\text{CuBi}_2\text{O}_4/\text{Ag}_3\text{PO}_4$ -SC and $\text{CuBi}_2\text{O}_4/\text{Ag}_3\text{PO}_4$ -SS, respectively.

The UV-Vis absorption spectra of the as-synthesized samples are shown in Figure 3a. Both pure Ag_3PO_4 -SC and Ag_3PO_4 -SS can absorb visible light with wavelengths higher than 500 nm, and pure CuBi_2O_4 shows the largest absorbing boundary higher than 800 nm. When the heterojunction structure forms between Ag_3PO_4 and CuBi_2O_4 , the composites $\text{CuBi}_2\text{O}_4/\text{Ag}_3\text{PO}_4$ -SC and $\text{CuBi}_2\text{O}_4/\text{Ag}_3\text{PO}_4$ -SS also exhibit intense absorption bands in the visible-light region. According to the Kubelka-Munk function [27] and the plot of $(\alpha h\nu)^2$ vs. $h\nu$ (shown in Figure 3b), the band gaps (E_g) of CuBi_2O_4 , Ag_3PO_4 -SC, and Ag_3PO_4 -SS can be estimated as 1.72 eV, 2.38 eV, and 2.42 eV, respectively. Besides, the band-edge potentials of the conduction band (E_{CB}) and valence band (E_{VB}) can be designated as [28]:

$$E_{VB} = X - E^C + 0.5E_g, \quad (1)$$

and

$$E_{CB} = X - E^C - 0.5E_g, \quad (2)$$

where X is the geometric mean of the electronegativity of the constituent atoms (5.96 eV for Ag_3PO_4 , and 4.59 eV for CuBi_2O_4 [28,29]), and E^C is the energy of the free electrons on the hydrogen scale (approximately 4.5 eV) [28]. Therefore, the E_{VB} and E_{CB} of CuBi_2O_4 can be estimated to be 0.95 and -0.77 eV/NHE, the E_{VB} and E_{CB} of Ag_3PO_4 -SC can be estimated to be 2.65 and 0.27 eV/NHE, while the E_{VB} and E_{CB} of Ag_3PO_4 -SS are estimated to be 2.67 and 0.25 eV/NHE, respectively.

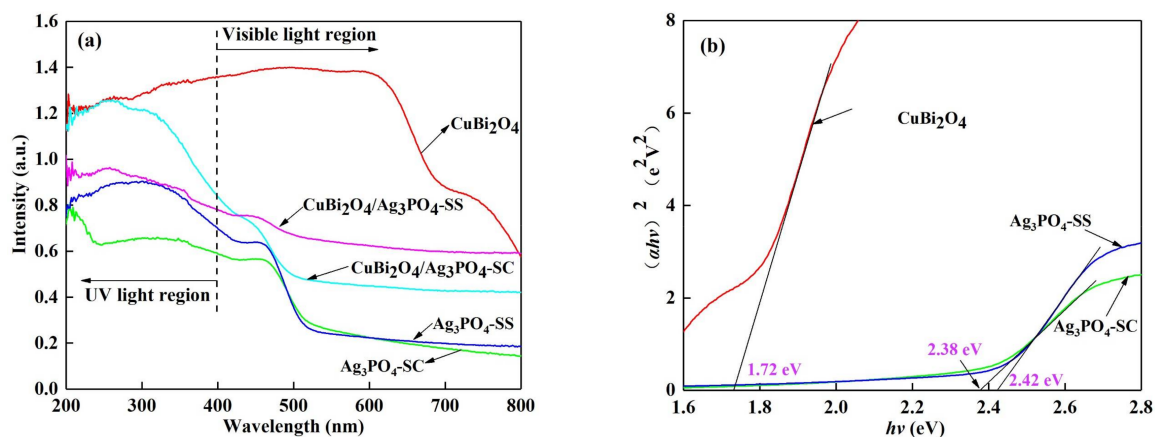


Figure 3. (a) UV-Vis diffuse reflectance spectra of the as-prepared materials, (b) band gap energy (E_g) of CuBi₂O₄, Ag₃PO₄-SC, and Ag₃PO₄-SS derived from the plots of $(ah\nu)^2$ versus energy ($h\nu$).

3.2. Photocatalytic Activity for DS Degradation

To evaluate the photocatalytic activity of the as-prepared catalysts, DS was selected as the target pollutant. Figure 4a shows the degradation efficiency of DS in different photocatalyst systems. In the system without any other catalysts, the degradation efficiency of DS is 36.87% under 300 min of visible light irradiation. As for the prepared catalysts, their adsorption efficiencies in the dark for DS are 1.76% (CuBi₂O₄), 0.30% (Ag₃PO₄-SC), 0.77% (Ag₃PO₄-SS), 3.36% (CuBi₂O₄/Ag₃PO₄-SC), and 6.98% (CuBi₂O₄/Ag₃PO₄-SS), respectively. This adsorption rule of catalysts is consistent with their specific surface area characteristics, whose data are displayed in Table 1; the specific surface area is an important parameter to evaluate the active adsorption sites of materials. Thus, the relatively lower adsorption efficiencies of as-prepared catalysts toward DS suggests the final removal rate of DS in the catalysts' system is mainly due to the photocatalysis. Under the same conditions, the degradation efficiencies of DS in CuBi₂O₄, Ag₃PO₄-SC, Ag₃PO₄-SS, CuBi₂O₄/Ag₃PO₄-SC, and CuBi₂O₄/Ag₃PO₄-SS systems are 63.98%, 72.55%, 76.87%, 83.75% and 90.68%, respectively. These results indicate that the addition of catalysts improves the photodegradation of DS and there is a synergy between CuBi₂O₄ and Ag₃PO₄.

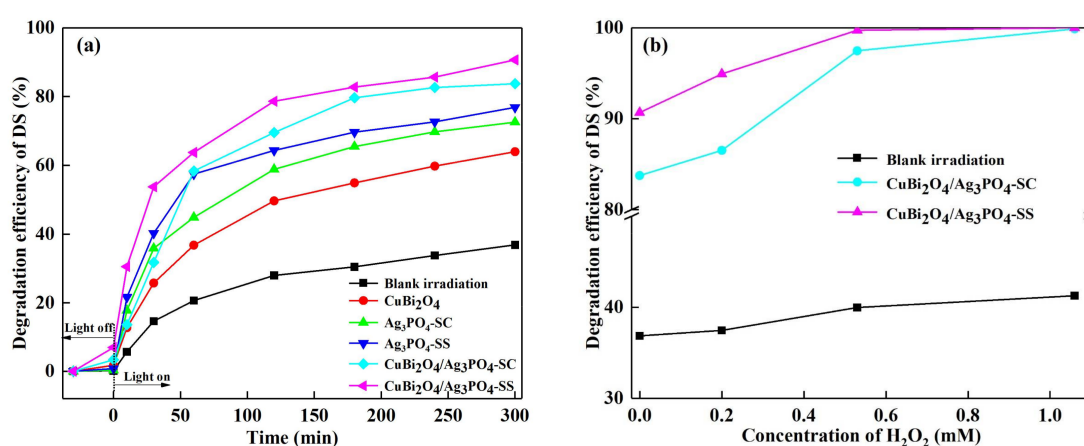


Figure 4. Cont.

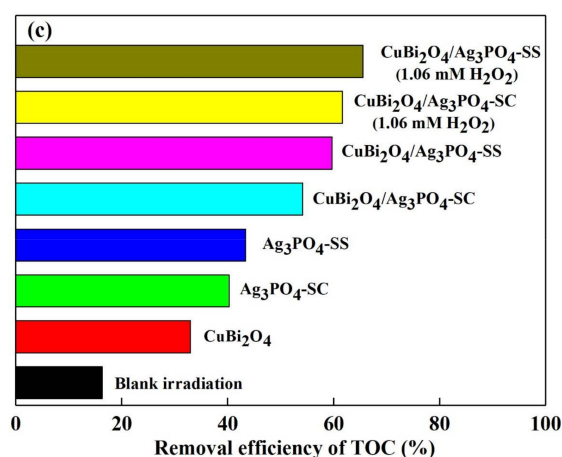


Figure 4. (a) Degradation efficiency of diclofenac sodium (DS) over different photocatalysts; (b) effect of H₂O₂ concentration on the removal efficiency of DS over CuBi₂O₄/Ag₃PO₄-SC and CuBi₂O₄/Ag₃PO₄-SS; (c) removal efficiency of TOC under different photocatalyst systems.

Table 1. Specific surface area of the as-prepared catalysts.

Samples	BET Surface Area (m ² g ⁻¹)
CuBi ₂ O ₄	2.307
Ag ₃ PO ₄ -SC	0.406
Ag ₃ PO ₄ -SS	0.984
CuBi ₂ O ₄ /Ag ₃ PO ₄ -SC	12.218
CuBi ₂ O ₄ /Ag ₃ PO ₄ -SS	14.596

Figure 4b shows the degradation efficiency of DS in different photocatalytic systems in the presence of H₂O₂. Overall, the degradation efficiency of DS increases with the increase of H₂O₂ concentration. When the concentration of H₂O₂ is 1.06 mM, the removal rate of DS in the blank irradiation system is 41.26%, which only improves by 4.39% of that without H₂O₂ (36.87%), showing no obvious effect of pure H₂O₂ on DS photodegradation. While for the CuBi₂O₄/Ag₃PO₄-SC and CuBi₂O₄/Ag₃PO₄-SS photocatalysts systems, the removal rates of DS achieve 97.48% and 99.73% when the concentration of H₂O₂ is 0.53 mM; in addition, the DS can be completely degraded when the concentration of H₂O₂ further increases to 1.06 mM. This reveals that there are synergistic effects between H₂O₂ and CuBi₂O₄/Ag₃PO₄ on the DS photodegradation.

In order to further demonstrate the synergistic promotion between CuBi₂O₄ and Ag₃PO₄, as well as H₂O₂ and CuBi₂O₄/Ag₃PO₄ for DS photodegradation, the mineralization rates of DS in the single CuBi₂O₄ or Ag₃PO₄ system, CuBi₂O₄/Ag₃PO₄ composite system, and the simultaneous presence system of H₂O₂ and CuBi₂O₄/Ag₃PO₄ were investigated. The experimental results are shown in Figure 4c. It can be clearly seen that mineralization rates of 16.27%, 32.97%, 40.23%, and 43.36% are obtained in the blank illumination, single CuBi₂O₄, Ag₃PO₄-SC, and Ag₃PO₄-SS systems, respectively. While under the same conditions, the mineralization rates of DS in CuBi₂O₄/Ag₃PO₄-SC and CuBi₂O₄/Ag₃PO₄-SS systems are 54.15% and 59.68%, respectively, which is an increase of 13.9% compared with that of the single catalyst system. In addition, the mineralization rates of DS in the CuBi₂O₄/Ag₃PO₄-SC and CuBi₂O₄/Ag₃PO₄-SS systems are further increased by 7.48% and 5.81% when the H₂O₂ concentration is 1.06 mM. These experimental results show the improvement of catalytic activity of CuBi₂O₄/Ag₃PO₄ composite in contrast with the single catalyst, and the further promotion effect of H₂O₂ on the catalytic activity of CuBi₂O₄/Ag₃PO₄ composite.

3.3. Photocatalytic Stability of the Catalysts

The stability of a photocatalyst is an important index to evaluate the value of its research value and actual utilization [30]. Therefore, we investigated the photocatalytic stability of CuBi_2O_4 , $\text{Ag}_3\text{PO}_4\text{-SC}$, $\text{Ag}_3\text{PO}_4\text{-SS}$, $\text{CuBi}_2\text{O}_4/\text{Ag}_3\text{PO}_4\text{-SC}$, $\text{CuBi}_2\text{O}_4/\text{Ag}_3\text{PO}_4\text{-SS}$, $\text{CuBi}_2\text{O}_4/\text{Ag}_3\text{PO}_4\text{-SC}$ (H_2O_2 , 1.06 mM) and $\text{CuBi}_2\text{O}_4/\text{Ag}_3\text{PO}_4\text{-SS}$ (H_2O_2 , 1.06 mM) using repeated experiments. The results described in Figure 5a show that the removal rates of DS in CuBi_2O_4 , $\text{Ag}_3\text{PO}_4\text{-SC}$, and $\text{Ag}_3\text{PO}_4\text{-SS}$ systems decrease by 4.62%, 11.42%, and 17.80% after four times recycling, indicating the poor stability of the single photocatalysts. While in the $\text{CuBi}_2\text{O}_4/\text{Ag}_3\text{PO}_4\text{-SC}$ and $\text{CuBi}_2\text{O}_4/\text{Ag}_3\text{PO}_4\text{-SS}$ composite systems, the removal rates of DS decrease by 6.31% and 12.32%, respectively. Compared with the single Ag_3PO_4 , the stability of the composite photocatalysts are improved to some extent. In addition, though the removal rates of DS are still decreased (decreased by 3.65% and 3.43%) when 1.06 mM H_2O_2 was added to the $\text{CuBi}_2\text{O}_4/\text{Ag}_3\text{PO}_4\text{-SC}$ and $\text{CuBi}_2\text{O}_4/\text{Ag}_3\text{PO}_4\text{-SS}$ systems, 96.24% and 95.02% of removal rates were obtained, which indicates that the addition of H_2O_2 greatly enhances the stability of $\text{CuBi}_2\text{O}_4/\text{Ag}_3\text{PO}_4$. The results depicted in Figure 5b show that the mineralization rates of DS for the fourth time recycled CuBi_2O_4 , $\text{Ag}_3\text{PO}_4\text{-SC}$, $\text{Ag}_3\text{PO}_4\text{-SS}$, $\text{CuBi}_2\text{O}_4/\text{Ag}_3\text{PO}_4\text{-SC}$, $\text{CuBi}_2\text{O}_4/\text{Ag}_3\text{PO}_4\text{-SS}$, $\text{CuBi}_2\text{O}_4/\text{Ag}_3\text{PO}_4\text{-SC}$ (H_2O_2 , 1.06 mM), and $\text{CuBi}_2\text{O}_4/\text{Ag}_3\text{PO}_4\text{-SS}$ (H_2O_2 , 1.06 mM) systems are 29.49%, 30.51%, 25.27%, 45.93%, 46.36%, 57.47%, and 59.73%, respectively. Compared with pure Ag_3PO_4 , it is a fact that the stability of the composite photocatalyst $\text{CuBi}_2\text{O}_4/\text{Ag}_3\text{PO}_4$ is improved, and the addition of H_2O_2 is helpful to further improve the photocatalytic stability of $\text{CuBi}_2\text{O}_4/\text{Ag}_3\text{PO}_4$.

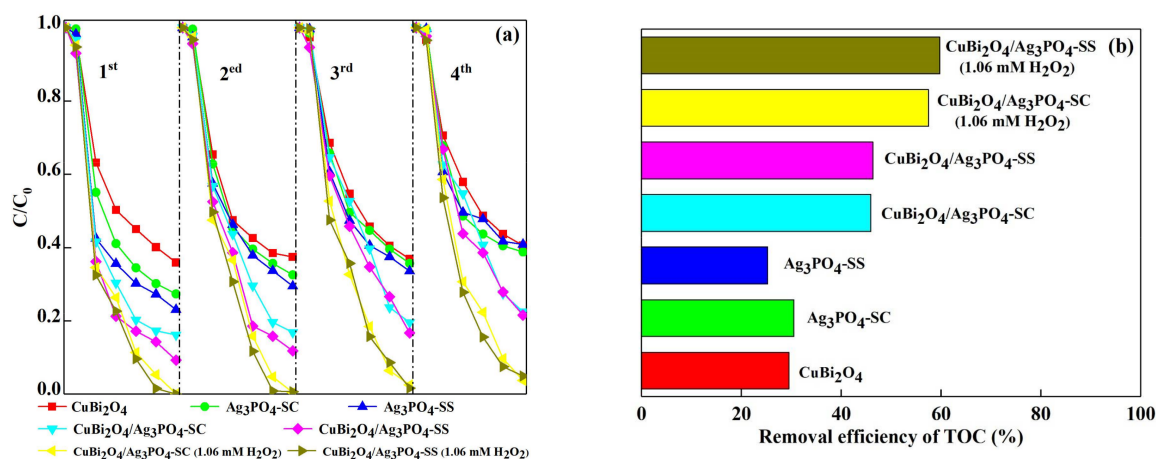


Figure 5. (a) Degradation efficiency of DS with different photocatalysts in different recycle runs; (b) TOC removal efficiency of the DS solution with four times recycling of photocatalysts.

The instability of the catalysts is mainly caused by the reduction of Ag^+ from the lattice of Ag_3PO_4 to generate Ag^0 during the reaction process. In order to analyze the photocatalytic stability of the as-prepared catalysts from the perspective of structure itself, XPS analysis of Ag3d for the fresh and reused catalysts was performed and the results are shown in Figure 6. It can be seen that, except for the Ag^+ peaks (374.17 eV and 368.16 eV) in the reused catalysts of $\text{Ag}_3\text{PO}_4\text{-SC}$ and $\text{CuBi}_2\text{O}_4/\text{Ag}_3\text{PO}_4\text{-SC}$, peaks indicating Ag^0 (374.40 eV and 368.32 eV) [31] are also observed, and the proportion of the peaks relative to Ag^0 occupy 11.38% and 9.52% of the total fitting peak area in the two catalysts. However, no obvious peaks relative to Ag^0 exist in the catalyst of $\text{CuBi}_2\text{O}_4/\text{Ag}_3\text{PO}_4\text{-SC}$ when 1.06 mM H_2O_2 was added into the reaction system. These results imply the enhanced stability of $\text{CuBi}_2\text{O}_4/\text{Ag}_3\text{PO}_4$ in comparison to pure Ag_3PO_4 , and again the further promotion of H_2O_2 for the composite's stability.

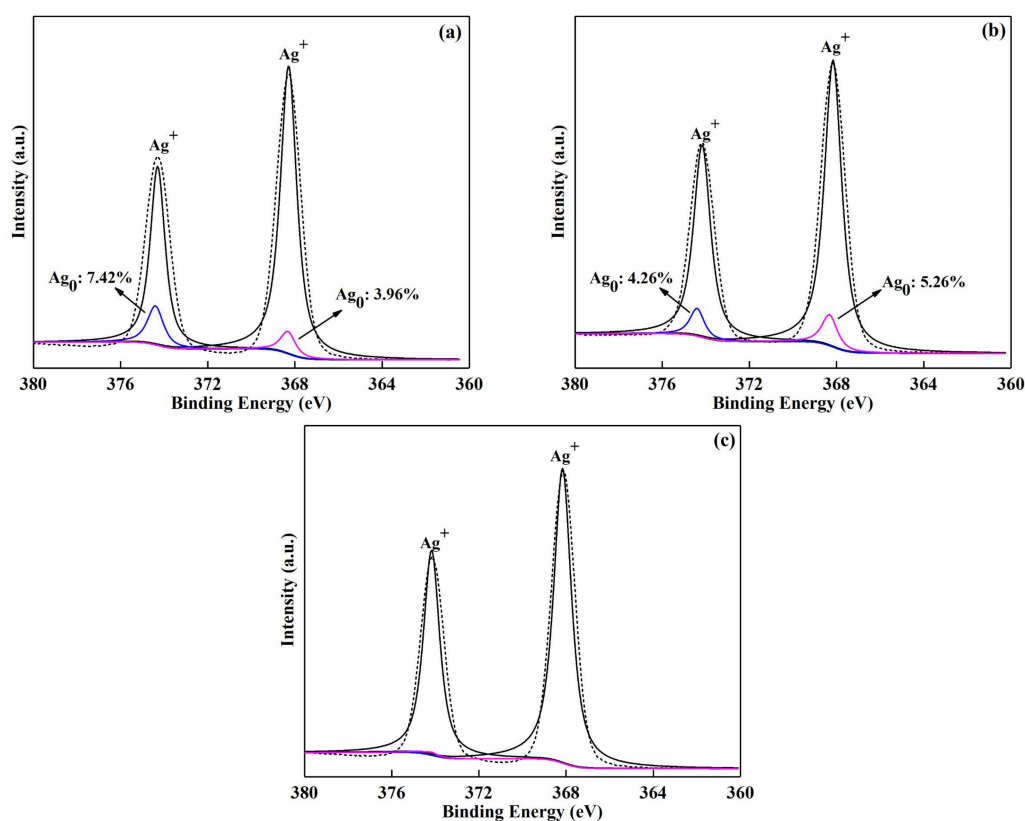


Figure 6. X-ray photoelectron spectra of Ag3d of the recycled photocatalysts, (a) Ag₃PO₄-SC; (b) CuBi₂O₄/Ag₃PO₄-SC; (c) CuBi₂O₄/Ag₃PO₄-SC (1.06 mM H₂O₂).

3.4. Photocatalytic Mechanism Discussion

Photoluminescence (PL) emission spectroscopy is important for understanding the photocatalytic mechanism of a catalyst by analyzing the migration and separation efficiency of photogenerated charge carriers in the material. Also, lower PL emission intensity implies a lower electron-hole recombination rate and corresponds to higher photocatalytic activity. Thus in this study, the PL emission spectra of the as-prepared catalysts were recorded under excitation at 500 nm, and the results are shown in Figure 7a. Compared with the pure CuBi₂O₄, Ag₃PO₄-SC, and Ag₃PO₄-SS, the composites CuBi₂O₄/Ag₃PO₄-SC and CuBi₂O₄/Ag₃PO₄-SS exhibit decreased emission intensity, suggesting the formation of the heterojunction between CuBi₂O₄ and Ag₃PO₄ decreases the recombination rate of electron-hole pairs. Moreover, the PL emission intensity rule of these catalysts is seriously coincident with that of the photocatalytic activity of the as-prepared materials.

Active species are important participants in photochemical reactions and they are also the key to discuss the photocatalytic mechanism. Thus, the free radical capture experiments were used to investigate whether OH•, h⁺, and O₂•⁻ are involved in the DS photodegradation process as well as their contribution order, while tert-butanol (*t*-BuOH), disodium ethylenediaminetetra-acetate (EDTA-Na₂), benzoquinone (BZQ) were chosen as the hydroxyl radical (OH•), hole (h⁺), superoxide radical (O₂•⁻) scavengers, respectively. The experiment results are shown in Figure 7b. For the CuBi₂O₄/Ag₃PO₄-SC and CuBi₂O₄/Ag₃PO₄-SS photocatalyst systems, the degradation efficiency of DS changed little when 1 mM Na₂-EDTA was added; while the degradation efficiency of DS decreased by 54.29% and 54.76% in the two catalyst systems when 1mM BZQ was added; when 2 mM *t*-BuOH was added, the degradation efficiency of DS decreased by 78.58% and 83.34%. This indicates that h⁺ does not participate in the degradation of DS in the CuBi₂O₄/Ag₃PO₄ photocatalyst systems, the active species involved in DS degradation are OH• and O₂•⁻, and the contribution order is OH• > O₂•⁻. Based on a similar

analysis mechanism, in the $\text{CuBi}_2\text{O}_4/\text{Ag}_3\text{PO}_4\text{-SC}$ and $\text{CuBi}_2\text{O}_4/\text{Ag}_3\text{PO}_4\text{-SS}$ photocatalysts systems with H_2O_2 , h^+ , OH^\bullet , and $\text{O}_2^{\bullet-}$ all involved in the degradation of DS, the contributions order is $\text{OH}^\bullet > h^+ > \text{O}_2^{\bullet-}$.

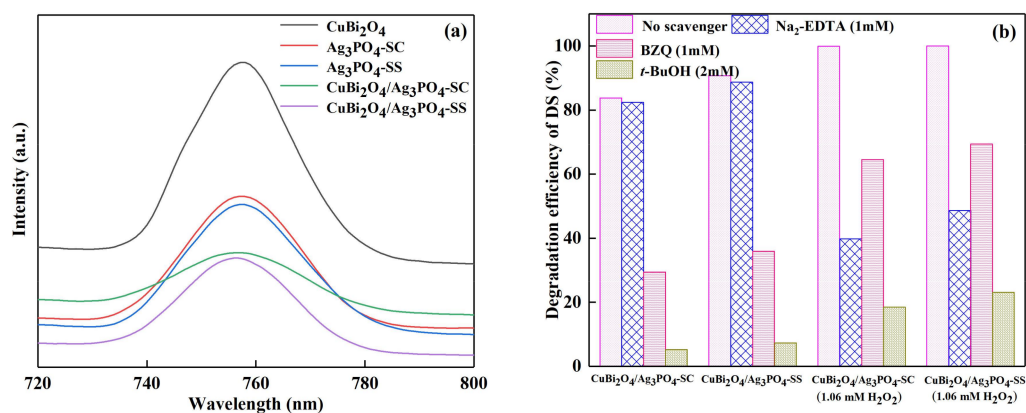


Figure 7. (a) Photoluminescence (PL) emission spectra of the as-prepared catalysts; (b) degradation efficiency of DS over different catalyst systems in the presence of scavengers.

Based on the above analysis, the photocatalytic mechanism of $\text{CuBi}_2\text{O}_4/\text{Ag}_3\text{PO}_4$ with or without H_2O_2 was discussed in detail. The following investigation only focuses on the catalyst $\text{CuBi}_2\text{O}_4/\text{Ag}_3\text{PO}_4\text{-SC}$ prepared using sodium citrate as the additive to discuss the effect of H_2O_2 on the photocatalytic mechanism of $\text{CuBi}_2\text{O}_4/\text{Ag}_3\text{PO}_4$. Figure 8a shows the migration pathways of the photogenerated electrons and holes of $\text{CuBi}_2\text{O}_4/\text{Ag}_3\text{PO}_4$ without H_2O_2 under visible light irradiation. As can be seen from the XPS spectrum of recycled $\text{CuBi}_2\text{O}_4/\text{Ag}_3\text{PO}_4$ (Figure 6b), Ag^0 has been formed on the surface of $\text{CuBi}_2\text{O}_4/\text{Ag}_3\text{PO}_4$ after reaction. Thus, the formed Ag^0 becomes the recombination center of h^+ coming from the valence band of CuBi_2O_4 and the e^- from the conduction band of Ag_3PO_4 , thereby promoting the separation of photogenerated h^+e^- pairs. In addition, e^- accumulated at the conduction band of CuBi_2O_4 can induce the generation of $\text{O}_2^{\bullet-}$, and h^+ accumulated at the valence band of Ag_3PO_4 can induce the generation of OH^\bullet ($E(\text{OH}^-/\text{OH}^\bullet) = 1.99$ eV [32]). The results of the free radical capture experiment show that the contribution of h^+ to DS degradation is small in the photocatalytic system using $\text{CuBi}_2\text{O}_4/\text{Ag}_3\text{PO}_4$ as catalyst, indicating that h^+ is mainly involved in the production of OH^\bullet and not involved in the degradation of DS. Therefore, the photocatalytic mechanism of $\text{CuBi}_2\text{O}_4/\text{Ag}_3\text{PO}_4$ is consistent with the Z-scheme theory described by Yu et al. [17,33] But as can be seen from Figure 8b, the photocatalytic mechanism of $\text{CuBi}_2\text{O}_4/\text{Ag}_3\text{PO}_4$ in the presence of H_2O_2 is more suitable to be explained by the heterojunction band theory [34]. That is, the electrons in the CB of CuBi_2O_4 can be transferred to the CB of Ag_3PO_4 easily, while the holes in the VB of Ag_3PO_4 can be transferred to the VB of CuBi_2O_4 due to the fact that both of the CB and VB positions of CuBi_2O_4 are higher than that of the Ag_3PO_4 , which promotes the separation of photogenerated h^+e^- pairs. Meanwhile, in the migration process of the photogenerated holes, the OH^- can be selectively oxidized to OH^\bullet by the holes ($E_{\text{VB}} = 2.65$ eV), which is due to the higher energy of holes than the standard redox potential of $E(\text{OH}^-/\text{OH}^\bullet) = 1.99$ eV (vs. NHE); while in the migration process of the photogenerated electrons, the O_2 adsorbed on the catalyst surface can be induced to generate $\text{O}_2^{\bullet-}$ [35], meanwhile, the e^- transforming into CB of Ag_3PO_4 ($E_{\text{CB}} = 0.27$ eV) can be easily be captured by the additive H_2O_2 for the generation of OH^\bullet ($E(\text{H}_2\text{O}_2/\text{OH}^\bullet) = 0.38$ eV) [36]. Therefore, OH^\bullet becomes the most important participant in DS degradation owing to its multi-channel sources, which is consistent with the results of the free radical capture experiment. In summary, the enhanced photocatalytic activity of $\text{CuBi}_2\text{O}_4/\text{Ag}_3\text{PO}_4$ by H_2O_2 is mainly due to the splitting of H_2O_2 to form much more effective OH^\bullet to degrade DS; and the enhanced stability of $\text{CuBi}_2\text{O}_4/\text{Ag}_3\text{PO}_4$

in the present of H_2O_2 is owing to the effective capture of photogenerated e^- by H_2O_2 , which greatly inhibits the reduction of Ag^+ from the lattice of Ag_3PO_4 .

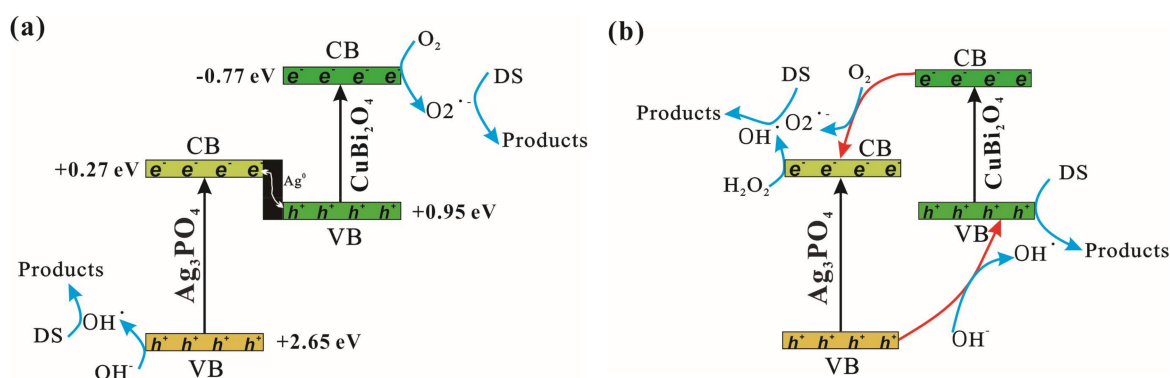


Figure 8. Schematic diagram for Eg matching and flow of photoinduced electrons/holes for (a) $\text{CuBi}_2\text{O}_4/\text{Ag}_3\text{PO}_4\text{-SC}$; (b) $\text{CuBi}_2\text{O}_4/\text{Ag}_3\text{PO}_4\text{-SC} (\text{H}_2\text{O}_2)$.

4. Conclusions

In this paper, two kinds of hetero-structural composite photocatalysts $\text{CuBi}_2\text{O}_4/\text{Ag}_3\text{PO}_4$ were prepared using sodium citrate or sodium stearate as additives. Under the same conditions, both of the two kinds of $\text{CuBi}_2\text{O}_4/\text{Ag}_3\text{PO}_4$ composites showed much improved excellent photocatalytic activity and stability than the single Ag_3PO_4 . Moreover, the addition of H_2O_2 further enhanced the photocatalytic performance of $\text{CuBi}_2\text{O}_4/\text{Ag}_3\text{PO}_4$. From the free radical capture experiments, the active species involved in DS degradation in the pure $\text{CuBi}_2\text{O}_4/\text{Ag}_3\text{PO}_4$ system are OH^\bullet and $\text{O}_2^{\bullet-}$, and the contribution order is $\text{OH}^\bullet > \text{O}_2^{\bullet-}$; while as H_2O_2 is added into the $\text{CuBi}_2\text{O}_4/\text{Ag}_3\text{PO}_4$ photocatalytic system, h^+ , OH^\bullet , and $\text{O}_2^{\bullet-}$ are all involved in the degradation of DS, and the contribution order is $\text{OH}^\bullet > h^+ > \text{O}_2^{\bullet-}$. Therefore, the catalytic mechanism of $\text{CuBi}_2\text{O}_4/\text{Ag}_3\text{PO}_4$ conforms to the Z-scheme theory; while the mechanism changes to heterojunction band theory after the addition of H_2O_2 .

Acknowledgments: This work was financially supported by the National Natural Science Foundation of China (grant number 51708116), the Scientific Research Foundation for High-level Talents of Foshan University (grant number gg07014), and Science and Technology Planning Project of Guangdong Province, China (grant number 2017B030314175).

Author Contributions: Xiaojuan Chen designed and performed the experiments, drafted the manuscript. Ning Li and Hailong Wang provided guidance for the general idea of the thesis. Song Xu and Yumin Cai carried out the sample preparations, part of the material characterization analysis, and data collection. All authors read and approved the final manuscript.

Conflicts of Interest: The authors declare no conflict of interest.

References

- Oliveira, T.D.; Guégan, R.; Thiebault, T.; Milbeau, C.L.; Muller, F.; Teixeira, V.; Giovanela, M.; Boussafir, M. Adsorption of diclofenac onto organoclays: Effects of surfactant and environmental (pH and temperature) conditions. *J. Hazard. Mater.* **2016**, *323*, 558–566. [[CrossRef](#)] [[PubMed](#)]
- Song, S.; Su, Y.; Adeleye, A.S.; Zhang, Y.; Zhou, X. Optimal design and characterization of sulfide-modified nanoscale zerovalent iron for diclofenac removal. *Appl. Catal. B Environ.* **2017**, *201*, 211–220. [[CrossRef](#)]
- Mezzelani, M.; Gorbi, S.; Fattorini, D.; d’Errico, G.; Consolandi, G.; Milan, M.; Bargelloni, L.; Regoli, F. Long-term exposure of *Mytilus galloprovincialis* to diclofenac, Ibuprofen and Ketoprofen: Insights into bioavailability, biomarkers and transcriptomic changes. *Chemosphere* **2018**, *198*, 238–248. [[CrossRef](#)] [[PubMed](#)]
- Vieno, N.; Sillanpää, M. Fate of diclofenac in municipal wastewater treatment plant—A review. *Environ. Int.* **2014**, *69*, 28–39. [[CrossRef](#)] [[PubMed](#)]

5. Sari, S.; Ozdemir, G.; Yangin-Gomec, C.; Zengin, G.E.; Topuz, E.; Aydin, E.; Pehlivanoglu-Mantas, E.; Okutman, T.D. Seasonal variation of diclofenac concentration and its relation with wastewater characteristics at two municipal wastewater treatment plants in Turkey. *J. Hazard. Mater.* **2014**, *272*, 155–164. [[CrossRef](#)] [[PubMed](#)]
6. Hu, X.X.; Xu, P.Q.; Cong, H.Y.; Yin, G.T. Synthesis and Characterization of WO₃/Graphene Nanocomposites for Enhanced Photocatalytic Activities by One-Step In-Situ Hydrothermal Reaction. *Materials* **2018**, *11*, 147–162.
7. Tran, H.T.T.; Kosslick, H.; Ibad, M.F.; Fischer, C.; Bentrup, U.; Vuong, T.H.; Nguyen, L.Q.; Schulz, A. Photocatalytic Performance of Highly Active Brookite in the Degradation of Hazardous Organic Compounds Compared to Anatase and Rutile. *Appl. Catal. B Environ.* **2017**, *200*, 647–658. [[CrossRef](#)]
8. Shi, L.; Wang, F.; Liang, L.; Chen, K.; Liu, M.; Zhu, R.; Sun, J. In site acid template induced facile synthesis of porous graphitic carbon nitride with enhanced visible-light photocatalytic activity. *Catal. Commun.* **2017**, *89*, 129–132. [[CrossRef](#)]
9. Chang, F.; Zheng, J.; Wang, X.; Xu, Q.; Deng, B.; Hu, X.; Liu, X. Heterojuncted non-metal binary composites silicon carbide/g-C₃N₄ with enhanced photocatalytic performance. *Mater. Sci. Semicond. Process.* **2018**, *75*, 183–192. [[CrossRef](#)]
10. Liang, Y.C.; Lo, Y.R.; Wang, C.C.; Xu, N.C. Shell Layer Thickness-Dependent Photocatalytic Activity of Sputtering Synthesized Hexagonally Structured ZnO-ZnS Composite Nanorods. *Materials* **2018**, *11*, 87. [[CrossRef](#)] [[PubMed](#)]
11. Martin, D.J.; Liu, G.; Moniz, S.J.; Bi, Y.; Beale, A.M.; Ye, J.; Tang, J. Efficient visible driven photocatalyst, silver phosphate: Performance, understanding and perspective. *Chem. Soc. Rev.* **2015**, *44*, 7808–7828. [[CrossRef](#)] [[PubMed](#)]
12. Chen, X.J.; Dai, Y.Z.; Guo, J.; Bu, F.Z.; Wang, X.Y. Synthesis of micro-nano Ag₃PO₄/ZnFe₂O₄ with different organic additives and its enhanced photocatalytic activity under visible light irradiation. *Mater. Sci. Semicond. Process.* **2016**, *41*, 335–342. [[CrossRef](#)]
13. Yi, Z.; Ye, J.; Kikugawa, N.; Kako, T.; Ouyang, S.; Stuartwilliams, H.; Yang, H.; Cao, J.; Luo, W.; Li, Z. An orthophosphate semiconductor with photooxidation properties under visible-light irradiation. *Nat. Mater.* **2010**, *9*, 559–564. [[CrossRef](#)] [[PubMed](#)]
14. Chen, X.J.; Dai, Y.Z.; Wang, X.Y. Methods and mechanism for improvement of photocatalytic activity and stability of Ag₃PO₄: A review. *J. Alloys Compd.* **2015**, *649*, 910–932. [[CrossRef](#)]
15. Zhao, G.Y.; Liu, L.J.; Li, J.R.; Liu, Q. Efficient removal of dye MB: Through the combined action of adsorption and photodegradation from NiFe₂O₄/Ag₃PO₄. *J. Alloys Compd.* **2016**, *664*, 169–174. [[CrossRef](#)]
16. Chen, Z.; Wang, W.; Zhang, Z.; Fang, X. High-Efficiency Visible-Light-Driven Ag₃PO₄/AgI Photocatalysts: Z-Scheme Photocatalytic Mechanism for Their Enhanced Photocatalytic Activity. *J. Phys. Chem. C* **2017**, *117*, 19346–19352. [[CrossRef](#)]
17. Shi, W.; Guo, F.; Yuan, S. In situ synthesis of Z-scheme Ag₃PO₄/CuBi₂O₄ photocatalysts and enhanced photocatalytic performance for the degradation of tetracycline under visible light irradiation. *Appl. Catal. B Environ.* **2017**, *209*, 720–728. [[CrossRef](#)]
18. Abroushan, E.; Farhadi, S.; Zabardasti, A. Ag₃PO₄/CoFe₂O₄ magnetic nanocomposite: Synthesis, characterization and applications in catalytic reduction of nitrophenols and sunlight-assisted photocatalytic degradation of organic dye pollutants. *RSC Adv.* **2017**, *7*, 18293–18304. [[CrossRef](#)]
19. Ren, J.; Chai, Y.; Liu, Q.; Zhang, L.; Dai, W.L. Intercorrelated Ag₃PO₄ nanoparticles decorated with graphitic carbon nitride: Enhanced stability and photocatalytic activities for water treatment. *Appl. Surf. Sci.* **2017**, *403*, 177–186. [[CrossRef](#)]
20. Chava, R.K.; Do, J.Y.; Kang, M. Fabrication of CdS-Ag₃PO₄ heteronanostructures for improved visible photocatalytic hydrogen evolution. *J. Alloys Compd.* **2017**, *727*, 86–93. [[CrossRef](#)]
21. Wang, F.; Yang, H.; Zhang, Y.; Wang, F.; Yang, H.; Zhang, Y.; Wang, F.; Yang, H.; Zhang, Y. Enhanced photocatalytic performance of CuBi₂O₄ particles decorated with Ag nanowires. *Mater. Sci. Semicond. Process.* **2018**, *73*, 58–66. [[CrossRef](#)]
22. Oh, W.D.; Dong, Z.; Lim, T.T. Hierarchically-structured Co-CuBi₂O₄ and Cu-CuBi₂O₄ for sulfanilamide removal via peroxymonosulfate activation. *Catal. Today* **2017**, *280*, 2–7. [[CrossRef](#)]

23. Nishikawa, M.; Yuto, S.; Hasegawa, T.; Shiroishi, W.; Hou, H.; Nakabayashi, Y.; Nosaka, Y.; Saito, N. Compositing effects of CuBi₂O₄ on visible-light responsive photocatalysts. *Mater. Sci. Semicond. Process.* **2017**, *57*, 12–17. [[CrossRef](#)]
24. Yin, H.; Cao, M.L.; Yu, X.X.; Li, C.; Shen, Y.; Zhu, M.Q. Hierarchical CuBi₂O₄ microspheres as lithium-ion battery anodes with superior high-temperature electrochemical performance. *RSC Adv.* **2017**, *7*, 13250–13256. [[CrossRef](#)]
25. Wang, F.; Chemseddine, A.; Abdi, F.F.; Krol, R.V.D.; Berglund, S.P. Spray pyrolysis of CuBi₂O₄ photocathodes: Improved solution chemistry for highly homogeneous thin films. *J. Mater. Chem. A* **2017**, *25*, 12838–12847. [[CrossRef](#)]
26. Zhang, Y.; Xie, Y.; Li, J.; Bai, T.; Wang, J. Photocatalytic activity and adsorption performance of p-CuBi₂O₄/n-TiO₂ p-n heterojunction composites prepared by in situ sol-gel coating method. *J. Sol Gel Sci. Technol.* **2014**, *71*, 38–42. [[CrossRef](#)]
27. Ming, G.; Na, Z.; Zhao, Y.; Jing, L.; Lu, L. Sunlight-Assisted Degradation of Dye Pollutants in Ag₃PO₄ Suspension. *Ind. Eng. Chem. Res.* **2012**, *51*, 5167–5173.
28. Eswar, K.R.; Katkar, V.V.; Ramamurthy, P.C.; Madras, G. Novel AgBr/Ag₃PO₄ Decorated Ceria Nanoflake Composites for Enhanced Photocatalytic Activity toward Dyes and Bacteria under Visible Light. *Ind. Eng. Chem. Res.* **2015**, *54*, 8031–8042. [[CrossRef](#)]
29. Patil, R.; Kelkar, S.; Naphade, R.; Ogale, S. Low temperature grown CuBi₂O₄ with flower morphology and its composite with CuO nanosheets for photoelectrochemical water splitting. *J. Mater. Chem. A* **2014**, *2*, 92–95. [[CrossRef](#)]
30. Martha, S.; Nashim, A.; Parida, K.M. Facile synthesis of highly active g-C₃N₄ for efficient hydrogen production under visible light. *J. Mater. Chem. A* **2013**, *1*, 7816–7824. [[CrossRef](#)]
31. Teng, W.; Li, X.; Zhao, Q.; Chen, G. Fabrication of Ag/Ag₃PO₄/TiO₂ heterostructure photoelectrodes for efficient decomposition of 2-chlorophenol under visible light irradiation. *J. Mater. Chem. A* **2013**, *1*, 9060–9068. [[CrossRef](#)]
32. Guo, J.; Ouyang, S.; Zhou, H.; Kako, T.; Ye, J. Ag₃PO₄/In(OH)₃ Composite Photocatalysts with Adjustable Surface-Electric Property for Efficient Photodegradation of Organic Dyes under Simulated Solar-Light Irradiation. *J. Phys. Chem. C* **2013**, *117*, 17716–17724. [[CrossRef](#)]
33. Zhou, P.; Yu, J.; Jaroniec, M. All-Solid-State Z-Scheme Photocatalytic Systems. *Adv. Mater.* **2014**, *26*, 4920–4935. [[CrossRef](#)] [[PubMed](#)]
34. Kanagaraj, T.; Thiripuranthagan, S. Photocatalytic activities of novel SrTiO₃-BiOBr heterojunction catalysts towards the degradation of reactive dyes. *Appl. Catal. B Environ.* **2017**, *207*, 218–232. [[CrossRef](#)]
35. Liu, W.; Wang, M.; Xu, C.; Chen, S.; Fu, X. Ag₃PO₄/ZnO: An efficient visible-light-sensitized composite with its application in photocatalytic degradation of Rhodamine B. *Mater. Res. Bull.* **2013**, *48*, 106–113. [[CrossRef](#)]
36. Su, M.; He, C.; Sharma, V.K.; Asi, M.A.; Xia, D.; Li, X.Z.; Deng, H.; Xiong, Y. Mesoporous zinc ferrite: Synthesis, characterization, and photocatalytic activity with HO/visible light. *J. Hazard. Mater.* **2012**, *211–212*, 95–103. [[CrossRef](#)] [[PubMed](#)]

